Supplemental Figure 1

IP : α-Flag

vector Flag-RARγ

RA (0.2uM, 1hr) : + - +

α-HA (Ngn2)
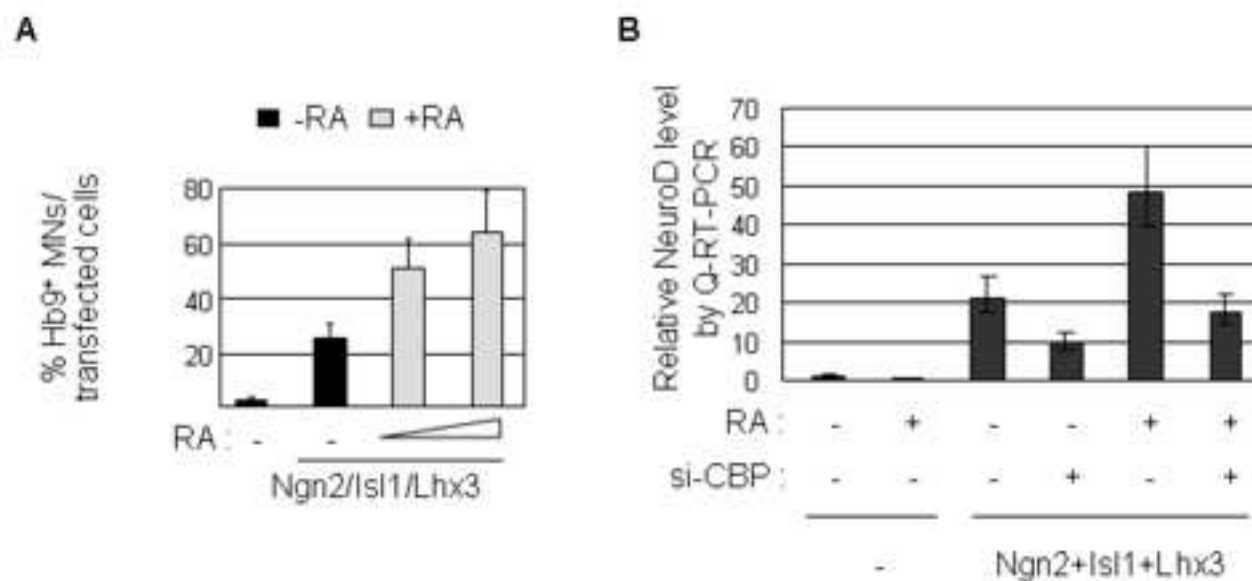
α-HA (Ngn2)

input

α-Flag ← RARγ

Supplemental Fig. 1: RARγ associates with RAR in cells. HEK293 cells transfected with HA-tagged Ngn2 and either Flag-vector or Flag-tagged RARγ were subjected to immunoprecipitation (IP) using anti-Flag antibody, followed by immunoblotting with anti-HA antibody. RARγ shows ligand-independent binding to Ngn2, like RARα. Interactions of Ngn2 with RARβ are also observed (data not shown).
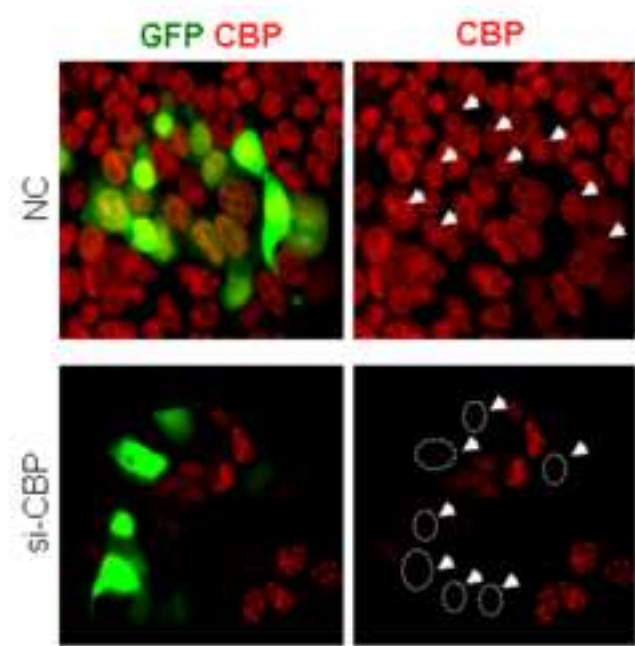
Supplemental Fig. 2: Down-regulation of CBP using si-CBP. Cells transfected with siRNA against CBP, marked by GFP, show decreased level of CBP (immunostained in red) relative to cells transfected with control siRNA (NC).
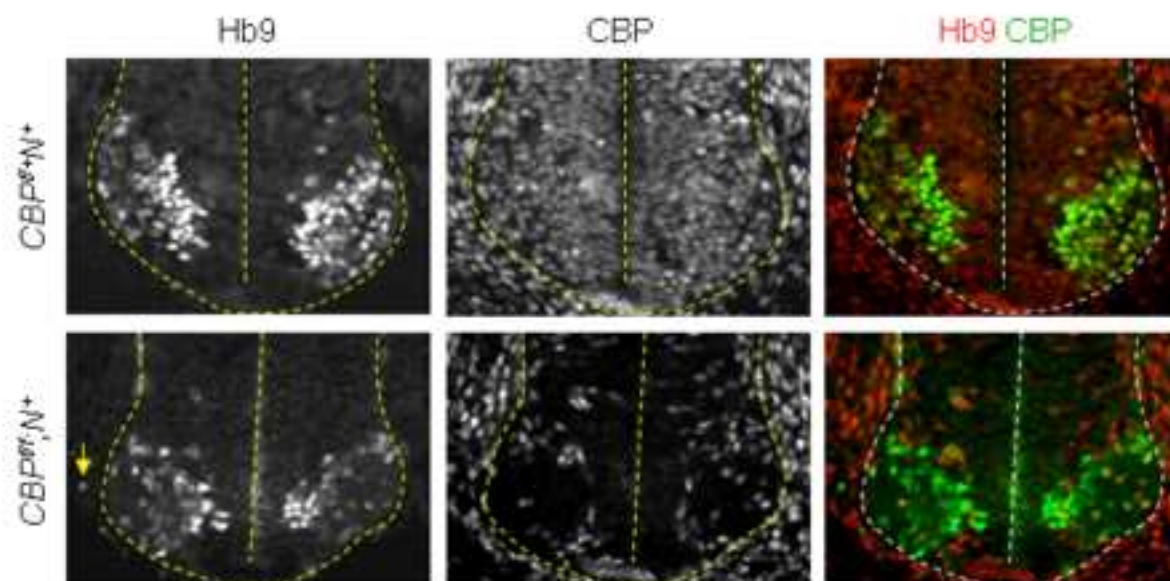
Supplemental Figure 3

A

■ -RA □ +RA

% Hb9⁺ MNs/ transfected cells

RA : -   -   ⟋

Ngn2/Isl1/Lhx3

B

Relative NeuroD level by Q-RT-PCR

RA :   -   +   -   -   +   +

si-CBP :   -   -   -   +   -   +

-          Ngn2+Isl1+Lhx3

Supplemental Fig. 3: Roles for RA in motor neuron differentiation of P19 cells. (A) RA enhances the ability of Ngn2, Isl1 and Lhx3 to induce motor neuron differentiation of P19 cells in a dose-dependent manner. (B) RA further stimulates expression of neuronal gene *NeuroD* in P19 cells transfected with Ngn2, Isl1 and Lhx3, as monitored by quantitative RT-PCR. Down-regulation of CBP using si-CBP attenuates the upregulation of NeuroD. The error bars represent the standard deviation.
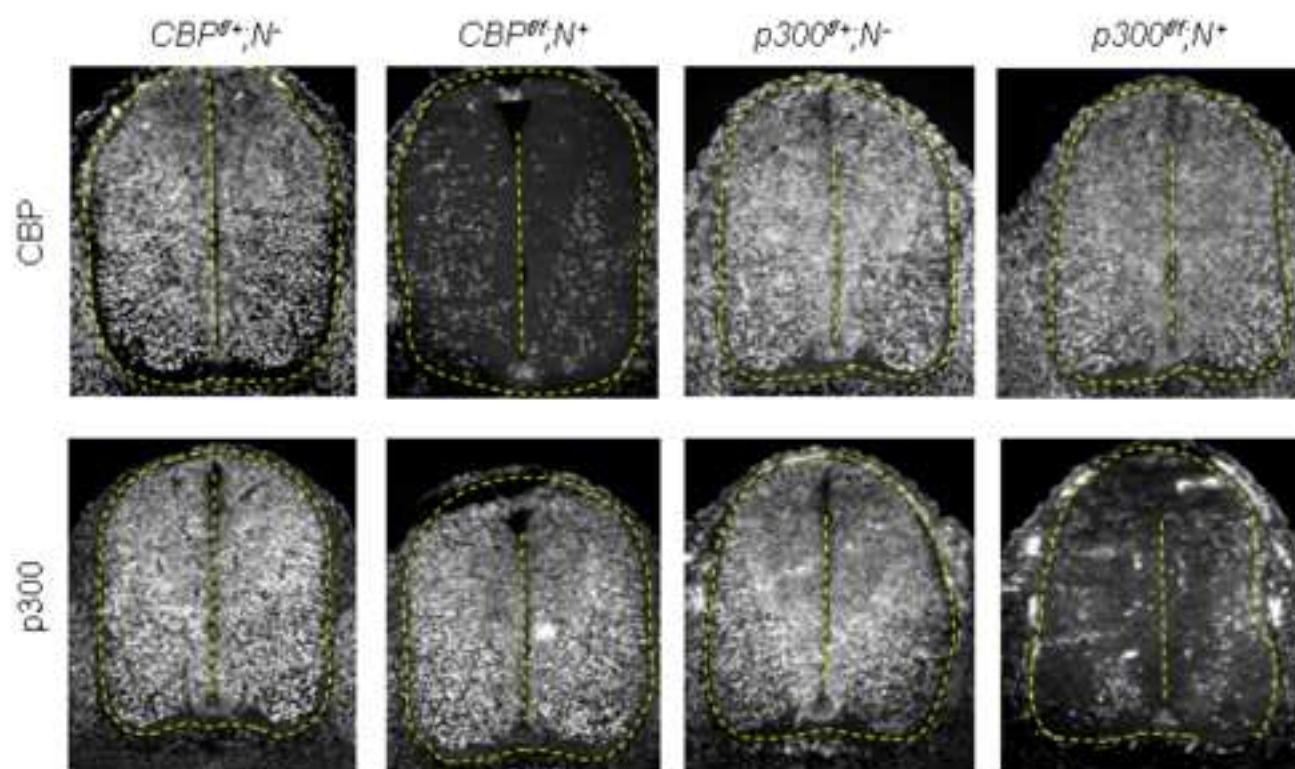
Supplemental Fig. 4: Specific inactivation of *CBP* and *p300* in *CBP^{ff};N^+* and *p300^{ff};N^+* embryos. Immunostaining with α-CBP and α-p300 antibodies reveal that nestin-promoter-directed expression of Cre-recombinase results in downregulation of CBP and p300, respectively, in the neural tube at E12.0. N denotes *nestin-Cre*.
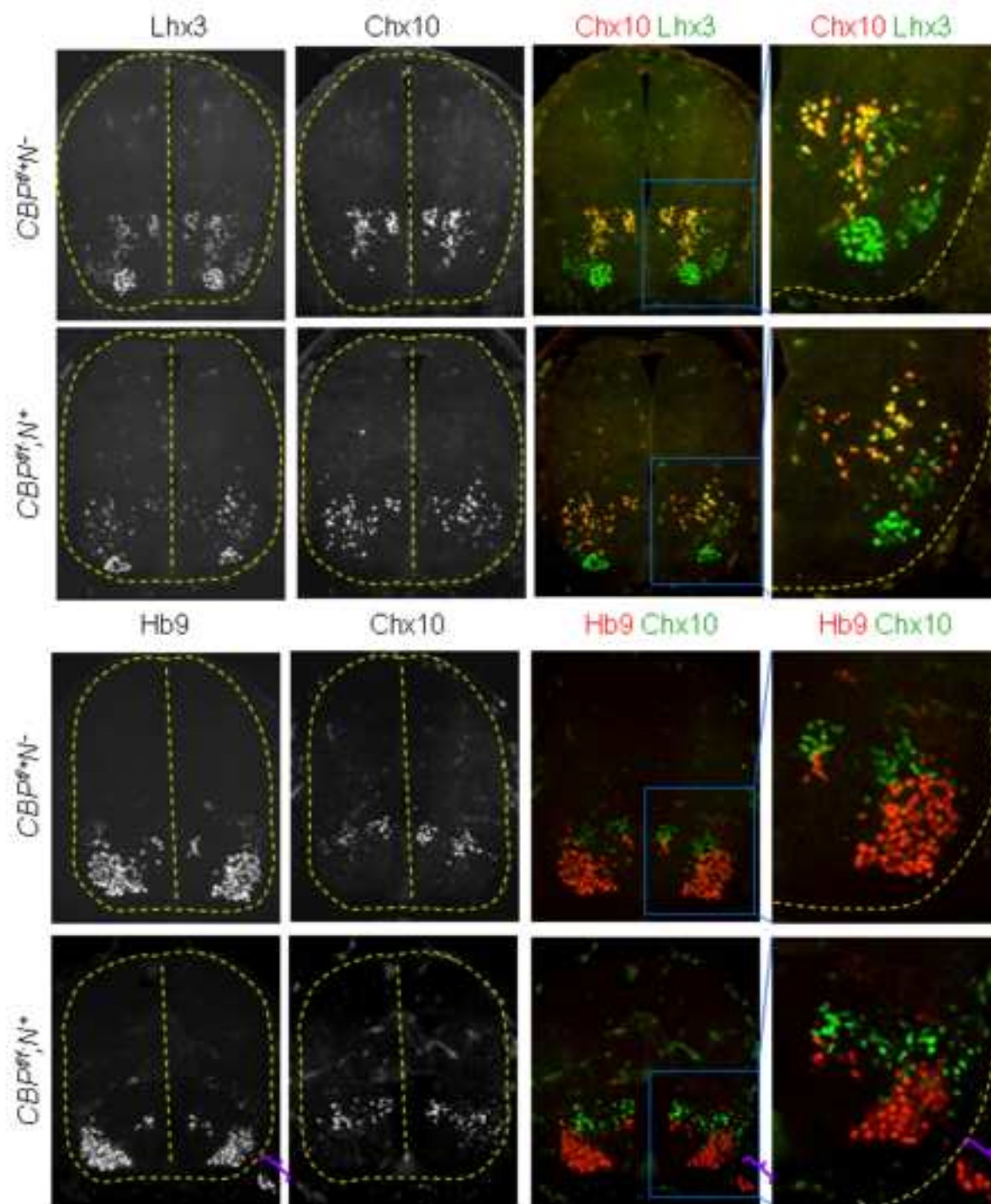
Supplemental Figure 5
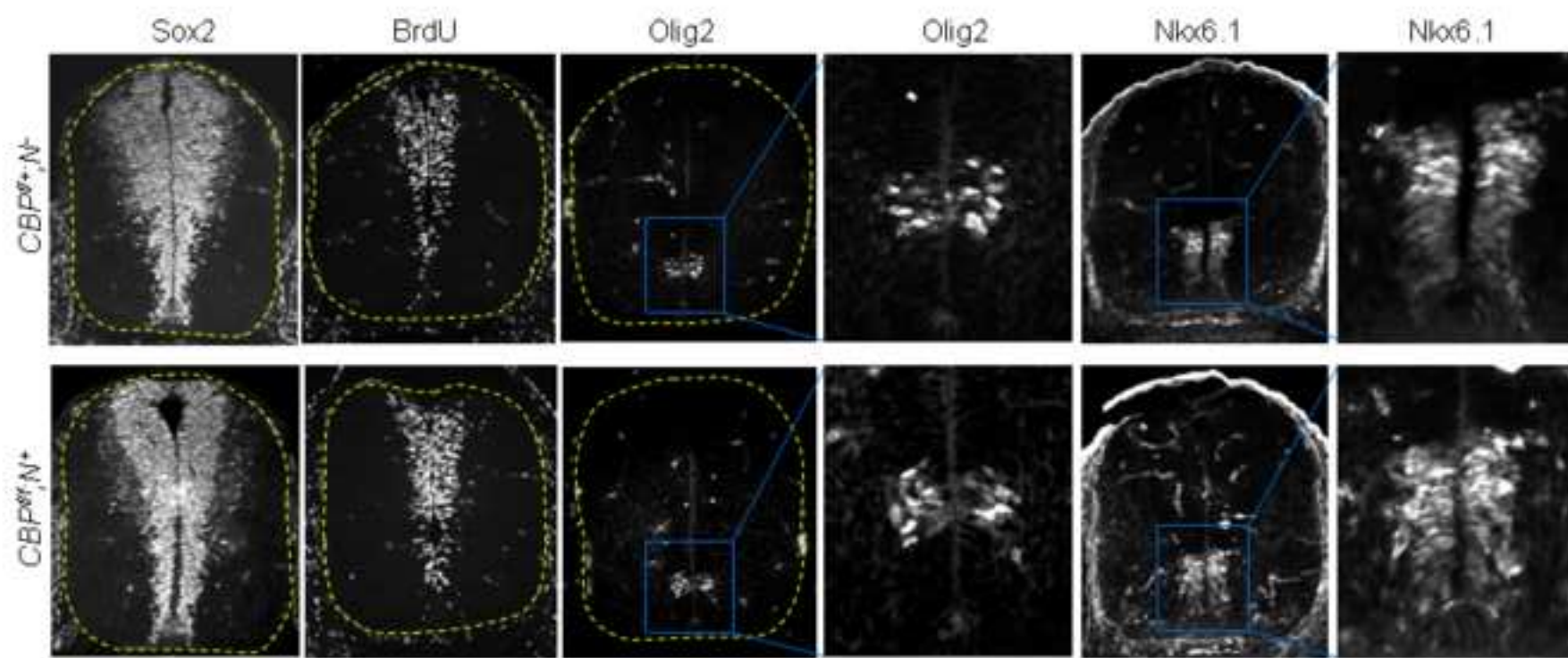
Supplemental Fig. 5: Immunostaining analyses in E12.0 *CBP* mutants. Spinal cord is outlined.

Supplemental Fig. 6: Immunostaining analyses at cervical level in E10.5 *CBP* mutants. The ventral spinal cord is shown, as outlined. The number of Hb9+ motor neurons is reduced in *CBP^ff^,N*+ embryos, in which CBP expression is greatly reduced. An extra-spinal motor neuron is marked by an arrow.
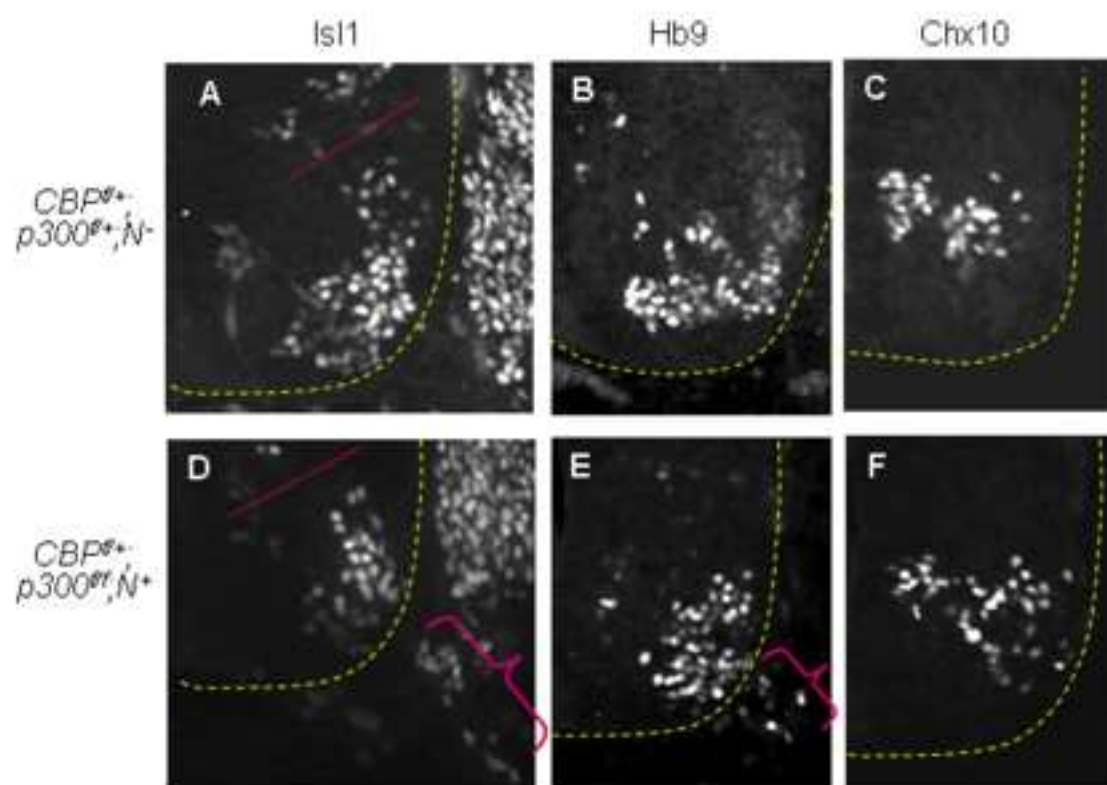
Supplemental Figure 7
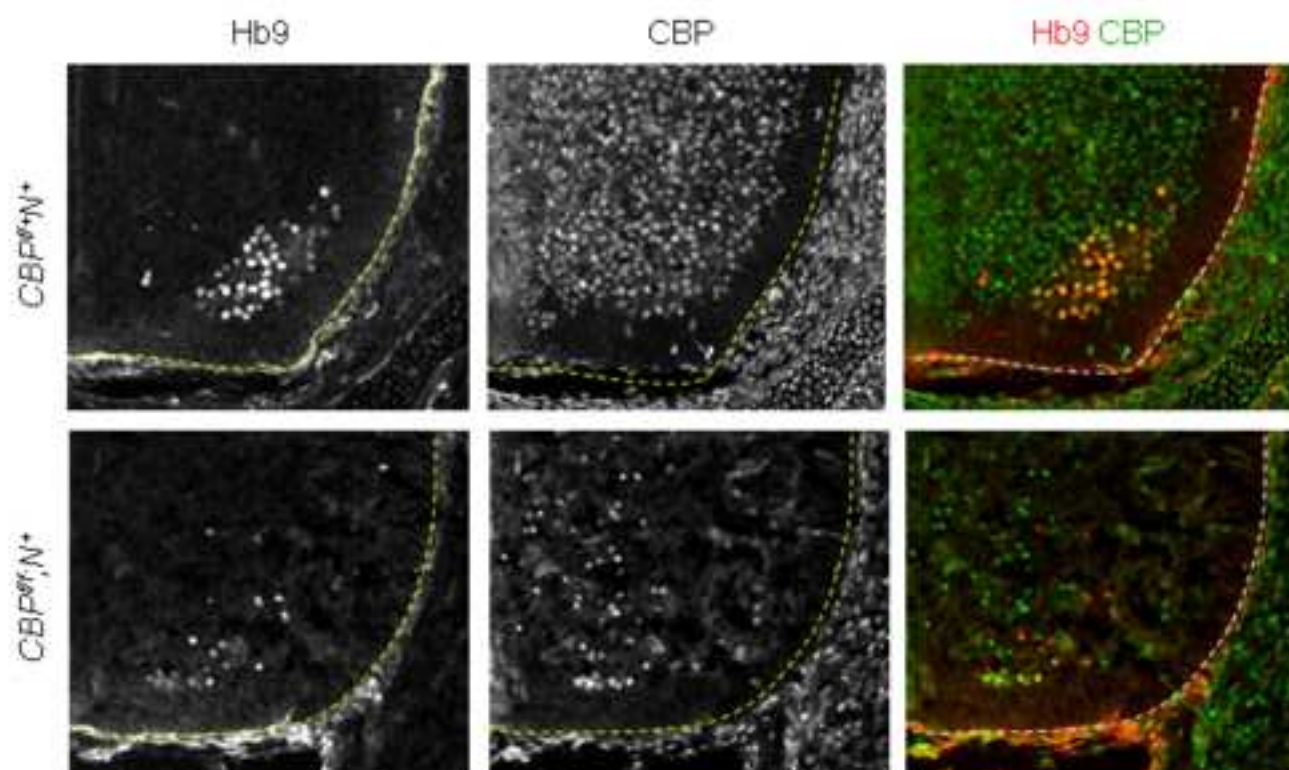
Supplemental Fig. 7: Immunostaining analyses at cervical level in E13.5 *CBP* mutants. A ventral quadrant of the spinal cord is shown, as outlined. The number of Hb9* motor neurons is reduced in *CBP^f/f^;N+* embryos, in which CBP expression is greatly reduced.

Lee_S-Fig. 8

Supplemental Fig. 8:
Immunostaining analyses in E12.0 *CBP* mutants. Spinal cord is outlined. The number of Hb9⁺Lhx3⁺ motor neurons is reduced in *CBP^ff;N⁺* embryos. Some motor neuron somata are mislocated outside the spinal cord (parenthesis). Interestingly, Chx10⁺ V2a-interneurons are more scattered ventro-laterally in *CBP^ff;N⁺* mutants.
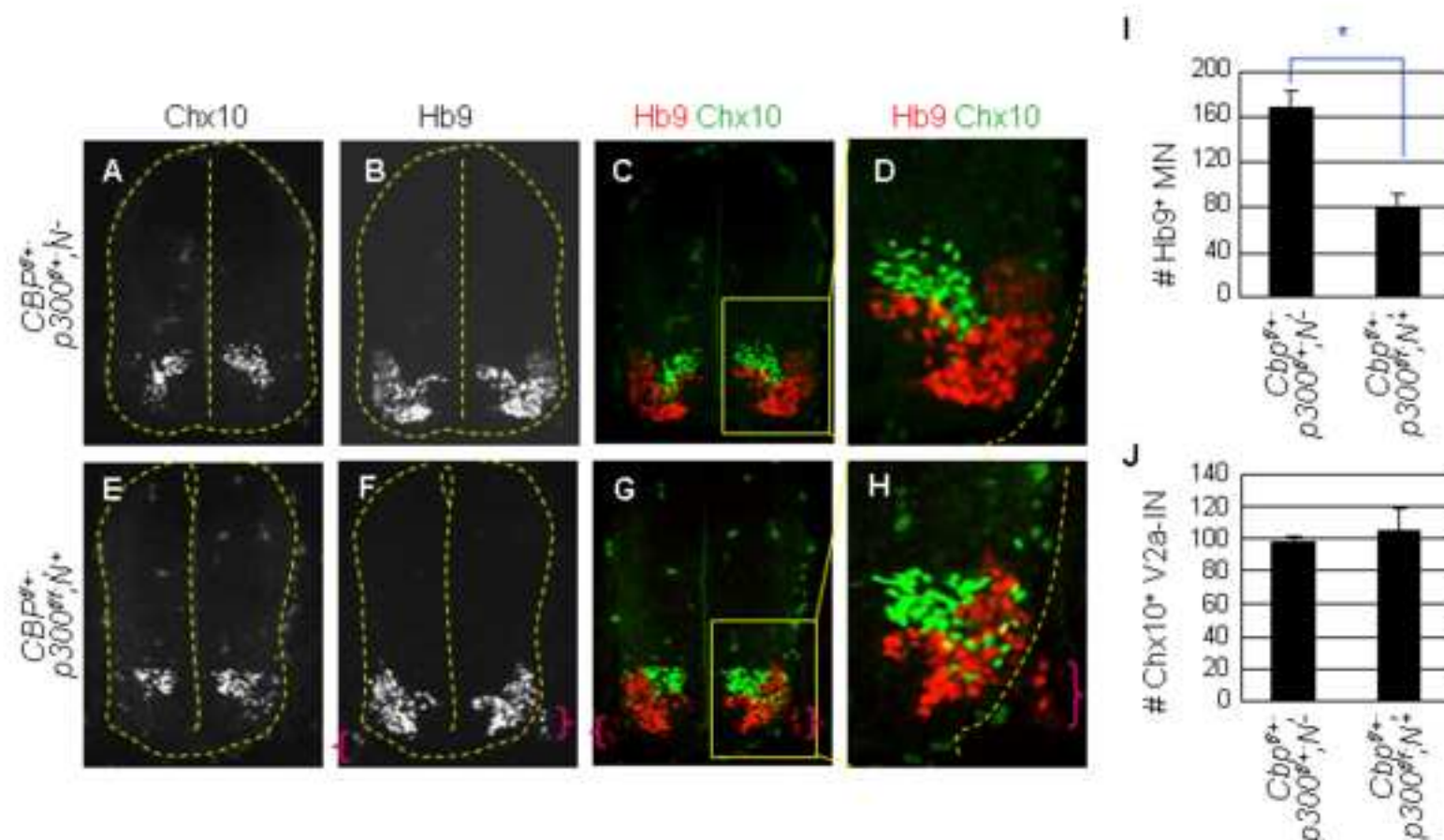
Supplemental Fig. 9: In E11.5 $Cbp^{f/+};p300^{f/f};N^+$ embryo, Hb9+ motor neurons are reduced to ~47% of control littermate ($CBP^{f/+};p300^{f/+};N^-$), and some motor neurons are migrated out of the spinal cord (parentheses in F, G, H). Interestingly, Chx10+ V2a-interneurons (V2a-INs) do not significantly change in numbers, but they are more scattered ventro-latereally. (I, J) Y-axis shows the number of neurons in 12 μm spinal cord sections. Asterisk, p<0.001 in the two-tailed t-test. The error bars represent the standard deviation.

Supplemental Fig. 10: Immunostaining analyses in E12.0 *CBP/p300* mutants. A ventral quadrant of the spinal cord is shown, as outlined. The number of Hb9+Isl1+ motor neurons is markedly reduced in *CBP^fl+;p300^fl;N+* embryos. Several Hb9+Isl1+ motor neuron somata are mislocated outside the spinal cord (parenthesis in D, E). Cell bodies of Chx10+ V2a-interneurons are located more ventro-laterally in *CBP^fl+;p300^fl;N+* mutants (compare C and F). Lines divide regions for motor neurons (lower part) and dorsal interneurons (upper part) (A, D).

CBP^ff,N^-   CBP^ff,N^+
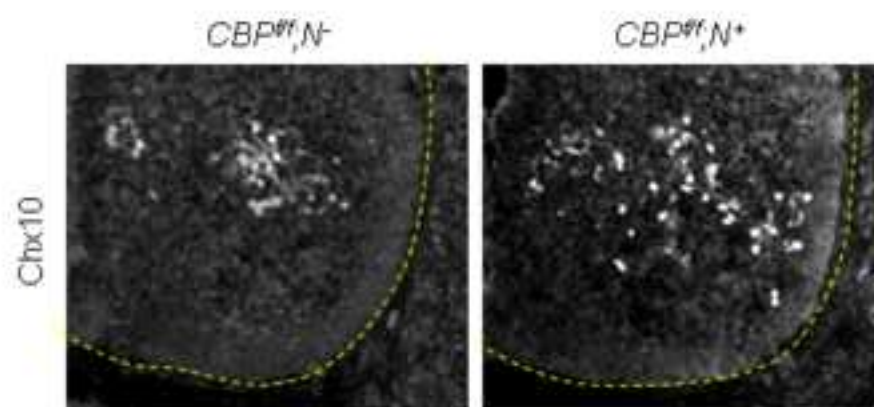
Chx10

Supplemental Fig. 11: Immunostaining analyses at thoracic level in E13.5 *CBP* mutants. A quadrant of the spinal cord is shown, as outlined. The Chx10+ V2a-interneurons are more scattered ventro-latereally.
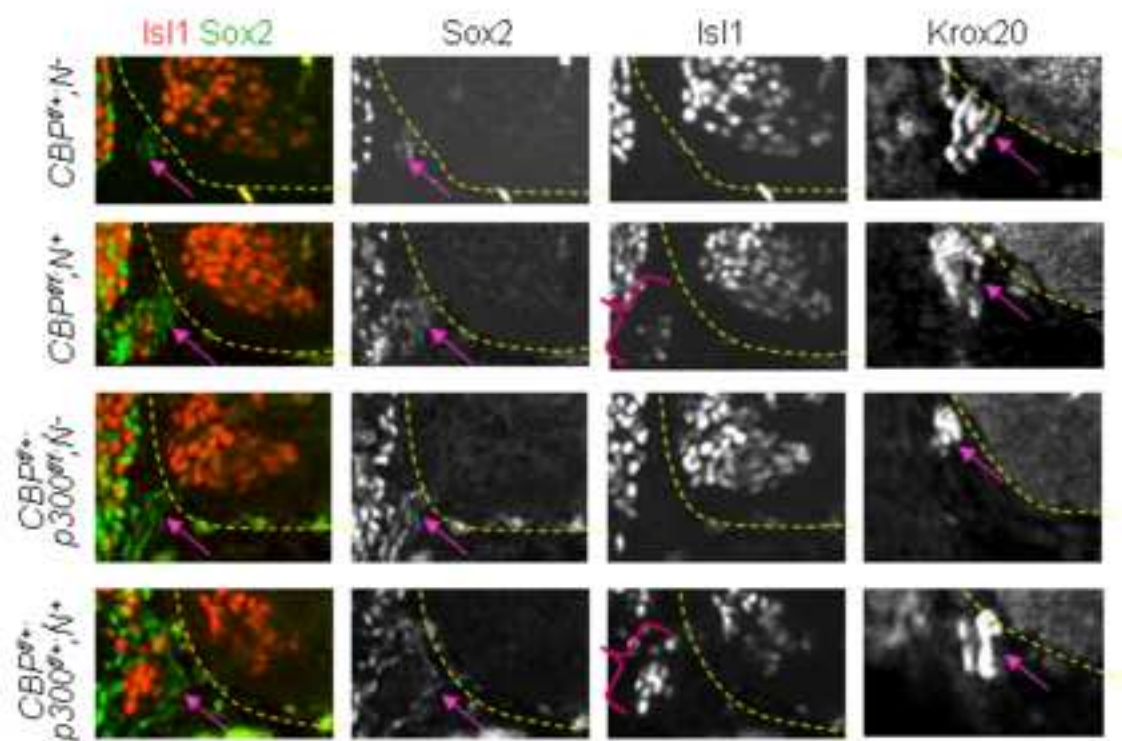
Supplemental Fig. 12: Boundary cap cells were properly formed in E12.0 *CBP/p300* mutants at the motor exit point, as determined by the boundary cap cell markers Krox20 and Sox2 (arrows). Parentheses mark emigrating Isl1+ motor neurons outside the spinal cord.
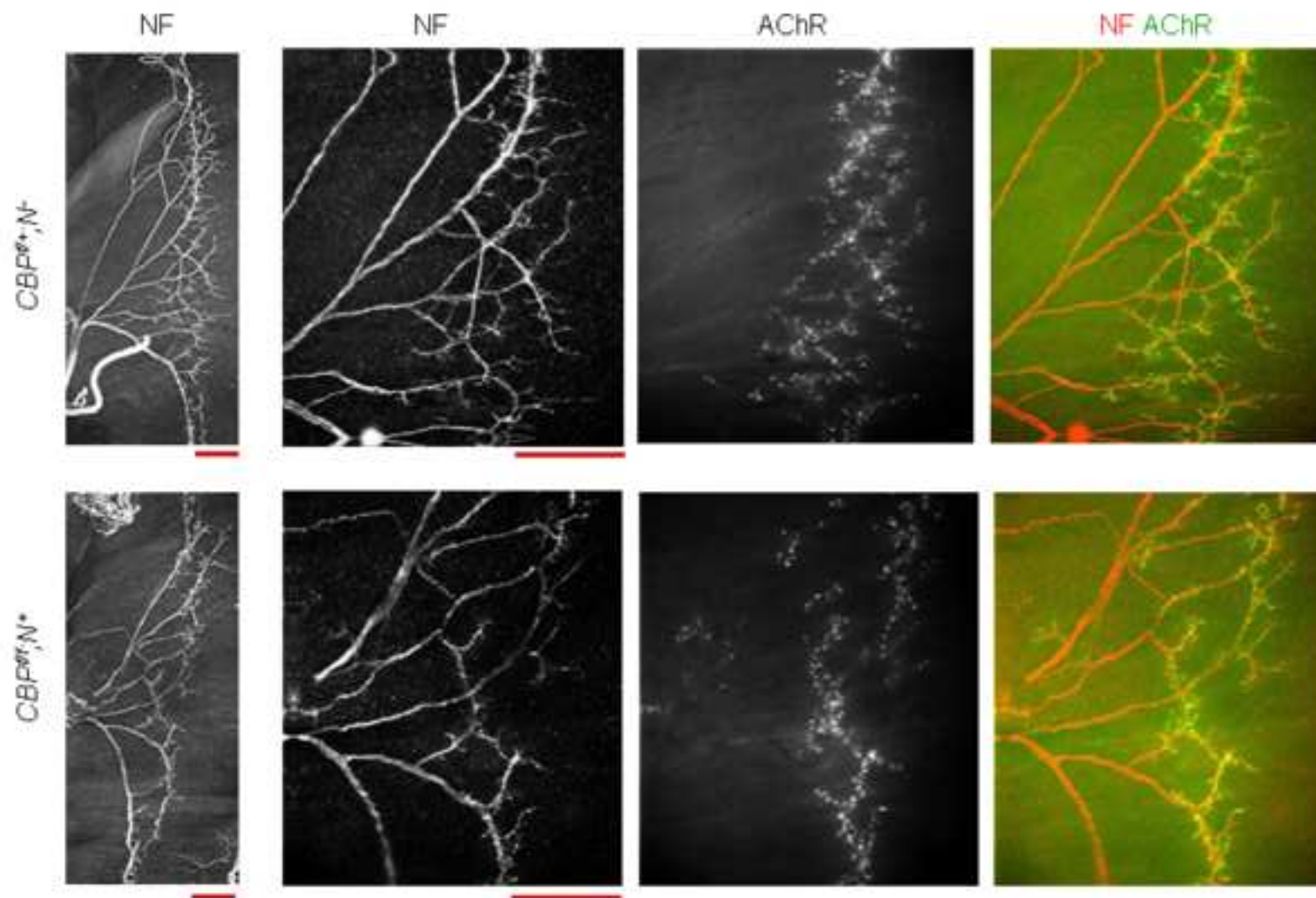
Supplemental Fig. 13: Whole mount staining of diaphragm muscle from E17.5 *CBP^{fl+};N$^-$* and *CBP^{fl};N$^+$* embryos. Motor axons of *CBP^{fl};N$^+$* embryo project for shorter distance from the main nerve and they are much less branched. In addition, the neuromuscular junction marked by the clustering of acetylcholine receptors (AChRs) are less organized in *CBP^{fl};N$^+$* embryos. Motor axons and AChRs are visualized by labeling with anti-neurofilament (NF) antibody and anti-bungarotoxin (BTX). Scale bar, 200 μm.

SUPPLEMENTAL EXPERIMENTAL PRODEDURES

DNA constructs and reagents

Mouse Lhx3, Ngn2 wild-type and Ngn2-AQ mutant (Ngn2-NR123,124AQ), CBP; human RARα, aa 1-432), RARα$^{\Delta AF2}$ (aa 1-374), RARα^{DBDmt} (point mutant C58A), RARα$^{DBDmt\Delta AF2}$ (C58A within aa 1-374), RARβ, RARγ and p300; rat Isl1 and nuclear LacZ were cloned into pCS2 and/or pcDNA3 (Invitrogen) containing a hemaglutinin (HA)-, myc- or flag-epitope tag. Luciferase reporter constructs MNe:LUC and E-box:LUC; mammalian expression vectors Ngn2-ires-GFP, E1A and E1AΔN have been described previously (Lee et al., 2001; Lee et al., 2004; Lee et al., 2005; Lee and Pfaff, 2003). DD-Isl1-Lhx3 is a triple fusion of the dimerization domain of NLI with the C-terminal ends of Isl1 and Lhx3 (Thaler et al., 2002). si-CBP duplex RNA (Santa cruz, sc-29243) and scrambled duplex RNA (Santa cruz, sc-44230) were used to knock-down CBP.

Antibodies

The following antibodies were used for immunohistochemistry, immunoprecipitation, and immunoblotting assays: rabbit anti-Hb9 (Thaler et al., 1999), goat anti-VAChT (Chemicon), guinea pig anti-Isl2 (Thaler et al., 2004), guinea pig anti-Chx10, rabbit anti-Lhx3, rabbit anti-Isl1 (Tsuchida et al., 1994), goat anti-Sox2 (Santa cruz, sc-17320), rabbit anti-neurofilament (Cappel), rabbit anti-Krox20 (Covance), rabbit anti-CBP (Santa-cruz, sc-369), rabbit anti-p300 (Santa-cruz, sc-584), mouse anti-HA (BabCo), mouse anti-Flag (Sigma), rabbit anti-RAR (Santa-cruz, sc-551), mouse anti-TuJ1 (Babco), mouse anti-histone3-lysine-4-trimethylation (abcam, ab8580-100), mouse anti-histone3-lysine-9-dimethylation (Upstate, 07-441), mouse anti-acetylated histone3/4 (Upstate, 06-599, 06-866), rat anti-BrdU (abcam, ab6326-250), rabbit anti-Olig2 (Novitch et al., 2001), mouse anti-Nkx6.1 (DSHB, F55A10) and mouse/rabbit IgG (Santa Cruz).

Transfections, luciferase assays, and P19 cell differentiation assays

P19 embryonic carcinoma cells were cultured in α-minimal essential media supplemented with 2.5% fetal bovine serum and 7.5% bovine calf serum. For luciferase assays, cells were seeded and incubated for 24 hr, and transient transfections were performed using Lipofectamine 2000 (Invitrogen). An actin promoter-β-galactosidase plasmid was cotransfected for normalization of transfection efficiency, and empty vectors were used to equalize the total amount of DNA. Cells were harvested 36-40 hr after transfection. 100 nM all-trans-retinoic acid (Sigma) or vehicle was treated for 16 hr prior to harvest. Cell extracts were assayed for luciferase activity and the values were normalized with β-galactosidase activity. Data are represented as means of triplicate values obtained from represented experiments. Histograms show mean normalized luciferase units and error bars represent standard deviation. All transfections were repeated independently at least four times.

For P19 cell differentiation assays, P19 cells were transfected using Lipofectamine 2000 (Invitrogen) and analyzed three days post-transfection by quantitative RT-PCR or immunohistochemistry. 0.5-1 μM all-trans-retinoic acid (Sigma) or vehicle was treated for 48hr prior to cell harvest. Total RNA was extracted with mini-kit (QIAGEN) and reverse transcription (RT) was performed using Superscript III (Invitrogen). The levels of mRNA were determined using quantitative RT-PCR (Mx3000P, Stratagene).

Following primers were used for RT-PCR: *Hb9* gene forward, 5'-CCA AGA TGC CGG ACT TCA G, reverse, 5'-TGC TGC GTT TCC ATT TCA TTC; *Neurofilament M* gene forward, 5'-CGA GAT GGT GAA CCA CGA GAA G, reverse, 5'-GTT CTG GTC TGA GTG ACA CTC G; *NeuroD* gene forward, 5'-CTT GAA GCC ATG AAT GCA GAG G, reverse,5'-AGA GCG TCT GTA CGA AGG AGA C

In ovo electroporation and quantification of fluorescence intensity

In ovo electroporation were performed as described (Thaler et al., 1999). Briefly, plasmid DNA was injected into the lumen of the neural tube of HH stage 13 chick embryos which

2

were then electroporated. The embryos were harvested at HH stage 20-26, fixed in 4% paraformaldehyde, embedded in OCT and cryosectioned at 12-18 µm. Co-electroporation of three plasmids typically resulted in greater than 90% of cells coexpressing both plasmids. More than 15 embryos were analyzed for each electroporation experiments and over 90% of embryos produced the identical/similar results along the rostral-caudal spinal cord. The pixel intensity of GFP and TuJ fluorescence in unsaturated images was determined using Axiovision software (Zeiss). The average pixel intensity from six readings was read across medial to lateral neural tube. Error bars indicate the standard deviations.

Immunohistochemistry

Immunohistochemistry was performed as described previously (Thaler et al., 1999). For neuromuscular junction visualization, diaphragm was dissected from heavily fixed E17.5 embryos and incubated with rabbit anti-neurofilament (Cappel), and FITC–conjugated α-bungarotoxin (α-BTX) (Molecular Probes), overnight at 4°C, as described previously (Thaler et al., 1999).

Co-immnoprecipitation (CoIP) assays

CoIP was performed as described previously (Joshi et al.) in P19 mouse carcinoma cells or human embryonic kidney 293 cells. Briefly, cells were harvested in lysis buffer (20mM Tris-HCl, pH8.0, 0.5% NP-40 and protease inhibitors) and incubated with antibodies overnight at 4°C. 20ul of Protein A/G-Sepharose was then added to the lysates and incubated at 4°C for 2hr. Beads were then washed with lysis buffer and the complexes were evaluated by western blotting. 100-200 nM all-trans-retinoic acid (Sigma) or vehicle was treated for 1-2 hr prior to cell harvest.

Chromatin immunoprecipitation (ChIP) assays

ChIP was performed as described previously (Joshi et al., 2009; Lee and Pfaff, 2003) in P19

cells or mouse embryonic spinal cord cells. P19 cells were transfected using Lipofectamine 2000 (Invitrogen) and analyzed two days post-transfection. 100 nM all-trans-retinoic acid (Sigma) or vehicle was treated for 2 hr prior to cell harvest. The spinal cords were micro-dissected from E12.5 mouse embryos and cells were dissociated and subject to ChIP assays. Following primers were used for ChIP: MNe in the mouse *Hb9* gene forward, 5'-GCA ACA CTT CCA GGC TCA GCC AG, reverse, 5'-CTG TTC TTG CAG ACT AGC AGG; β-RARE in the mouse *RARβ2* gene forward, 5'-CTG CTG GGA GTT TTT AAG C, reverse, 5'-GGC AAA GAA TAG ACC CTC C.

References

Joshi, K., Lee, S., Lee, B., Lee, J. W., and Lee, S. K. LMO4 reinforces cell fate choices between V2a and V2b interneurons in the developing spinal cord. Submitted to Nat Neurosci.

Lee, S. K., Jung, S. Y., Kim, Y. S., Na, S. Y., Lee, Y. C., and Lee, J. W. (2001). Two distinct nuclear receptor-interaction domains and CREB-binding protein-dependent transactivation function of activating signal cointegrator-2. Mol Endocrinol *15*, 241-254.

Lee, S. K., Jurata, L. W., Funahashi, J., Ruiz, E. C., and Pfaff, S. L. (2004). Analysis of embryonic motoneuron gene regulation: derepression of general activators function in concert with enhancer factors. Development *131*, 3295-3306.

Lee, S. K., Lee, B., Ruiz, E. C., and Pfaff, S. L. (2005). Olig2 and Ngn2 function in opposition to modulate gene expression in motor neuron progenitor cells. Genes Dev *19*, 282-294.

Lee, S. K., and Pfaff, S. L. (2003). Synchronization of neurogenesis and motor neuron specification by direct coupling of bHLH and homeodomain transcription factors. Neuron *38*, 731-745.

Novitch, B. G., Chen, A. I., and Jessell, T. M. (2001). Coordinate regulation of motor neuron subtype identity and pan-neuronal properties by the bHLH repressor Olig2. Neuron *31*, 773-789.

Thaler, J., Harrison, K., Sharma, K., Lettieri, K., Kehrl, J., and Pfaff, S. L. (1999). Active suppression of interneuron programs within developing motor neurons revealed by analysis of homeodomain factor HB9. Neuron *23*, 675-687.

Thaler, J. P., Koo, S. J., Kania, A., Lettieri, K., Andrews, S., Cox, C., Jessell, T. M., and Pfaff, S. L. (2004). A postmitotic role for Isl-class LIM homeodomain proteins in the assignment of visceral spinal motor neuron identity. Neuron *41*, 337-350.

Thaler, J. P., Lee, S. K., Jurata, L. W., Gill, G. N., and Pfaff, S. L. (2002). LIM factor Lhx3 contributes to the specification of motor neuron and interneuron identity through cell-type-specific protein-protein interactions. Cell *110*, 237-249.

Tsuchida, T., Ensini, M., Morton, S. B., Baldassare, M., Edlund, T., Jessell, T. M., and Pfaff, S. L. (1994). Topographic organization of embryonic motor neurons defined by expression of LIM homeobox genes. Cell *79*, 957-970.